

1 **Ensemble daily simulations for elucidating cloud-aerosol interactions under a large**
2 **spread of realistic environmental conditions**

3
4 **Guy Dagan¹ and Philip Stier¹**

5 ¹ Atmospheric, Oceanic and Planetary Physics, Department of Physics, University of Oxford, UK

6 E-mail: guy.dagan@physics.ox.ac.uk

7
8 **Abstract**

9 Aerosol effects on cloud properties and the atmospheric energy and radiation budgets are
10 studied through ensemble simulations over two month-long periods during the NARVAL
11 campaigns (December 2013 and August 2016). For each day, two simulations are conducted
12 with low and high cloud droplet number concentrations (CDNC), representing low and high
13 aerosol concentrations, respectively. This large data-set, which is based on a large spread of
14 co-varying realistic initial conditions, enables robust identification of the effect of CDNC
15 changes on cloud properties. We show that increases in CDNC drive a reduction in the top of
16 atmosphere (TOA) net shortwave flux (more reflection) and a decrease in the lower
17 tropospheric stability for all cases examined, while the TOA longwave flux and the liquid and
18 ice water path changes are generally positive. However, changes in cloud fraction or
19 precipitation, that could appear significant for a given day, are not as robustly affected, and, at
20 least for the summer month, are not statistically distinguishable from zero. These results
21 highlight the need for using large statistics of initial conditions for cloud-aerosol studies for
22 identifying the significance of the response. In addition, we demonstrate the dependence of the
23 aerosol effects on the season, as it is shown that the TOA net radiative effect is doubled during
24 the winter month as compared to the summer month. By separating the simulations into
25 different dominant cloud regimes, we show that the difference between the different months
26 emerge due to the compensation of the longwave effect induced by an increase in ice content
27 as compared to the shortwave effect of the liquid clouds. The CDNC effect on the longwave is
28 stronger in the summer as the clouds are deeper and the atmosphere is more unstable.

29
30
31
32
33

34 **Introduction**

35 Cloud droplets form on suitable aerosols which can serve as cloud condensation nuclei. Thus,
36 for vertical velocities which are sufficient to sustain aerosol activation, cloud droplet number
37 concentration (CDNC) increases with increasing aerosol concentrations. Concomitantly with
38 the increase in the CDNC, and assuming constant liquid water content, the initial cloud
39 hydrometeor (liquid and ice particles) size distribution shifts to smaller sizes and becomes
40 narrower, which may modulate cloud micro- and macro-physical properties (Khain et al.,
41 2005;Koren et al., 2005;Heikenfeld et al., 2019;Chen et al., 2017;Altaratz et al., 2014;Seifert
42 and Beheng, 2006a;Koren et al., 2014;Dagan et al., 2017;Dagan et al., 2018b), the rain
43 production (Levin and Cotton, 2009;Albrecht, 1989;Tao et al., 2012;Dagan et al., 2015b) and
44 the clouds' radiative effect (Koren et al., 2010;Storelvmo et al., 2011;Twomey, 1977;Albrecht,
45 1989). Anthropogenic aerosol emissions may thus perturb Earth's radiation budget both
46 directly, by scattering and absorption, and also indirectly, through these cloud-mediated
47 mechanisms. However, despite decades of effort of trying to better understand the processes
48 involved, cloud-aerosol interactions are still considered one of the most uncertain
49 anthropogenic effects on climate (Boucher et al., 2013).

50 The aerosol effect on clouds was previously shown to be cloud regime dependent (Altaratz et
51 al., 2014;Lee et al., 2009;Mülmenstädt and Feingold, 2018;van den Heever et al.,
52 2011;Rosenfeld et al., 2013;Glassmeier and Lohmann, 2016;Gryspeerd and Stier,
53 2012;Christensen et al., 2016). In addition, even for a given cloud regime, small changes in the
54 meteorological conditions may change the sign and magnitude of the aerosol effect (Dagan et
55 al., 2015b;Fan et al., 2009;Fan et al., 2007;Kalina et al., 2014;Khain et al., 2008;Liu et al.,
56 2019).

57 The fact that the aerosol effect on clouds and precipitation is dependent on the cloud regime
58 and meteorological conditions, makes the quantification of its global effect challenging and
59 uncertain (Mülmenstädt and Feingold, 2018;Bellouin et al., 2019). One way to overcome this
60 challenge is by examining the aerosol effect for an ensemble of realistic co-varying initial
61 conditions (as opposed to perturbing each environmental condition separately). This can be
62 done by conducting ensemble/routine numerical simulations (such as those conducted in
63 previous studies (Gustafson and Vogelmann, 2015;Gustafson et al., 2017;Klocke et al., 2017))
64 focusing on aerosol effects. This methodology enables identifying, using large statistics, clouds
65 and radiative properties that respond in a consistent manner to aerosol (noting that in a single-
66 case studies some of the differences between different simulations could be just due to different

67 realizations of the model (Grabowski, 2015)). This methodology also enables investigation of
68 the aerosol effect on cloud and precipitation as a function of the initial conditions.

69 In a recent paper, focusing on two specific cases (each one for two days) and a relatively large
70 domain ($22^\circ \times 11^\circ$), the physical processes controlling the aerosol effect on the atmospheric
71 energy budget were investigated (Dagan et al., 2019). It was shown that the total column
72 atmospheric radiative warming ($Q_R = (F_{SW}^{TOA} - F_{SW}^{SFC}) + (F_{LW}^{TOA} - F_{LW}^{SFC})$), defined as the rate of net
73 atmospheric diabatic warming due to radiative shortwave (SW) and longwave (LW) fluxes at
74 the surface (SFC) and top of the atmosphere (TOA), when all fluxes positive downwards), is
75 substantially increased with CDNC in a deep-cloud dominated case (by $\sim 10 \text{ W/m}^2$), while a
76 much smaller increase ($\sim 1.6 \text{ W/m}^2$) is shown in a shallow-cloud dominated case. This trend is
77 caused by an increase in the upward mass flux of ice and water vapor to the upper troposphere
78 that leads to reduced outgoing longwave radiation (Fan et al., 2012). The increase in mass flux
79 is caused partially by an increase in vertical velocities (Koren et al., 2005; Rosenfeld et al.,
80 2008; Dagan et al., 2018a) and mostly by an increase in the water content at the mid-troposphere
81 (due to warm rain suppression) that increases the upward mass flux, even for a give vertical
82 velocity. The change in net radiative fluxes at the TOA (F_{SW+LW}^{TOA}) was shown to be -5.2 W/m^2
83 for the shallow-cloud dominated case and -1.9 W/m^2 for the deep-cloud dominated case. Dagan
84 et al. (2019) also show that the cloud fraction responds in opposite ways to CDNC perturbations
85 in the different cases, increasing in the deep-cloud dominated case and decreasing in the
86 shallow-cloud dominated case. However, it is unclear how representative these results are as
87 they are based on two specific cases. The ensemble simulations presented in this study could
88 be used to examine the robustness of these aerosol effects using large statistics.

89 The focus of this study is on clouds over the Atlantic Ocean near Barbados (Fig. 1). Barbados
90 is located north of the mean intertropical convergence zone (ITCZ) location, in a way that
91 samples both the trade region, dominated by shallow cumulus during the boreal winter, and the
92 transition to deep convection as the ITCZ migrates northward during boreal summer (Stevens
93 et al., 2016). Hence, this location enables investigation of different cloud regimes and different
94 meteorological conditions. In addition, the clouds near Barbados have been shown to be
95 representative of clouds across the trade region (Medeiros and Nuijens, 2016).

96

97 **Methodology**

98 Ensemble daily simulations using the icosahedral nonhydrostatic (ICON) atmospheric model
99 (Zängl et al., 2015) in a limited area configuration are conducted. ICON's dynamical core has
100 been validated against several idealized cases as well as against numerical weather prediction

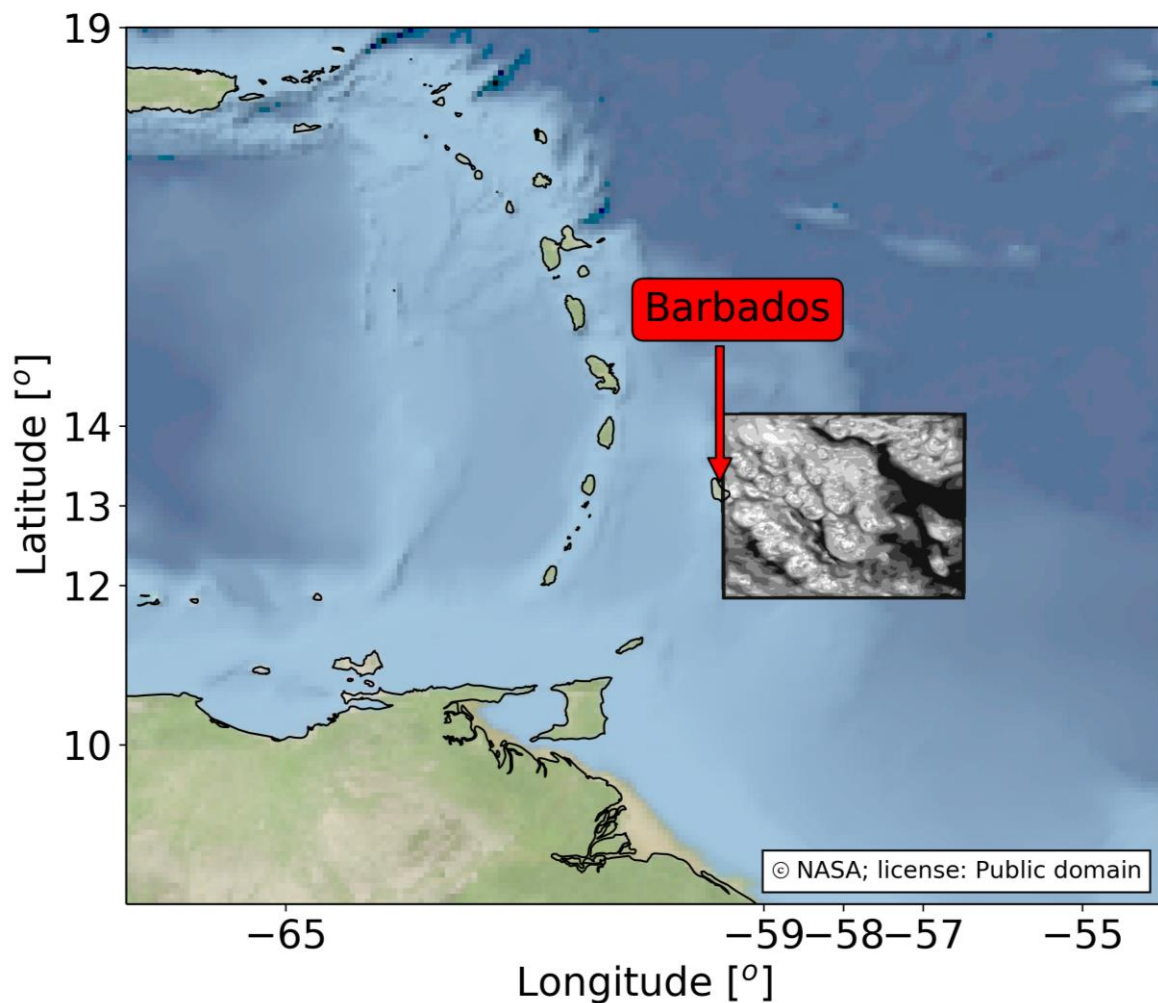
101 skill scores (Zängl et al., 2015). The domain is located east of Barbados island and covers $\sim 3^\circ$
102 $\times 3^\circ$ (Fig. 1). The simulations are aligned with the NARVAL (Next-generation Aircraft
103 Remote-Sensing for Validation Studies (Klepp et al., 2014;Stevens et al., 2019;Stevens et al.,
104 2016)) campaigns which took place during December 2013 (NARVAL 1) and August 2016
105 (NARVAL 2) in the northern tropical Atlantic. We use existing NARVAL convection-
106 permitting simulations (Klocke et al., 2017) as initial and boundary conditions for our
107 simulations and a two-moment bulk microphysical scheme (Seifert and Beheng, 2006b). For
108 each day during these two months, two different simulations are started with identical initial
109 conditions with different CDNC of 20 cm^{-3} (clean) and 200 cm^{-3} (polluted), resulting in an
110 ensemble of 124 simulations. The different CDNC scenarios serve as proxy for different
111 aerosol concentration conditions and are chosen as they represent the range typically observed
112 over the ocean (Rosenfeld et al., 2019;Gryspeerd et al., 2019). Using fixed CDNC avoids the
113 uncertainties involved in the representation of aerosol processes in numerical models
114 (Rothenberg et al., 2018), however, it limits potential feedbacks between clouds and aerosols,
115 such as through aerosol scavenging (Yamaguchi et al., 2017). In addition, we note that use of
116 a microphysical scheme which assumes saturation adjustment reduces the sensitivity of the
117 clouds to some of the aerosol effect (Koren et al., 2014; Dagan et al., 2015a; Heiblum et al.,
118 2016; Fan et al., 2018).

119 Each simulation is conducted for 24 hours, starting from 12 UTC - 12 hours after the original
120 simulations of Klocke et al., 2017 were initialized from reanalysis data, to reduce spin-up
121 effects. Using initial and boundary conditions based on ICON simulations with similar
122 resolution, as in Klocke et al. (2017), reduces the spin-up effects. The horizontal resolution is
123 set to 1200 m and 75 vertical levels are used. The temporal resolution is 12 seconds and the
124 output interval is 30 minutes. Interactive radiation is calculated every 12 minutes using the
125 RRTM-G scheme (Clough et al., 2005;Iacono et al., 2008;Mlawer et al., 1997). The simulations
126 include an interactive surface flux scheme and a fixed (for each day) sea surface temperature.
127 As in Dagan et al. (2019), the simulations include representation of the Twomey effect,
128 calculated with diagnosed cloud droplet effective radii from the microphysical scheme
129 (Twomey, 1977). However, due to the large uncertainty involved in the ice microphysics and
130 morphology, no Twomey effect due to changes in the ice particles size distribution was
131 considered.

132 In addition, the domain is setup to include the Barbados Cloud Observatory (BCO, (Stevens et
133 al., 2016)) while minimising the island effect of Barbados (most of the domain is east of the
134 island and only the east part of the island, which includes the BCO (13°N , 59°W), is included

135 in the domain). Observations from the BCO are used for model evaluation (Figs. S1 and S2,
136 supporting information), and demonstrate that the model performs well for low surface-SW-
137 flux days but underestimates the flux for high-SW-flux days (usually under low cloud fraction).
138 We note that although a $3^\circ \times 3^\circ$ domain is larger than the domains used in many previous
139 studies, it is still possible that the use of fixed boundary conditions for the different simulations
140 under different CDNC conditions reduces some of the sensitivity as compared to simulations
141 with larger domains such as in Dagan et al. (2019) ($22^\circ \times 11^\circ$).

142



143

144 **Figure 1.** The domain of the simulations (the box in the middle) and the area around it. Inside the domain
145 is presented the average cloud fraction over the first 30 mins of the simulation for 1/8/2016, CDNC = 20
146 cm^{-3} . The island of Barbados is marked with a red arrow.

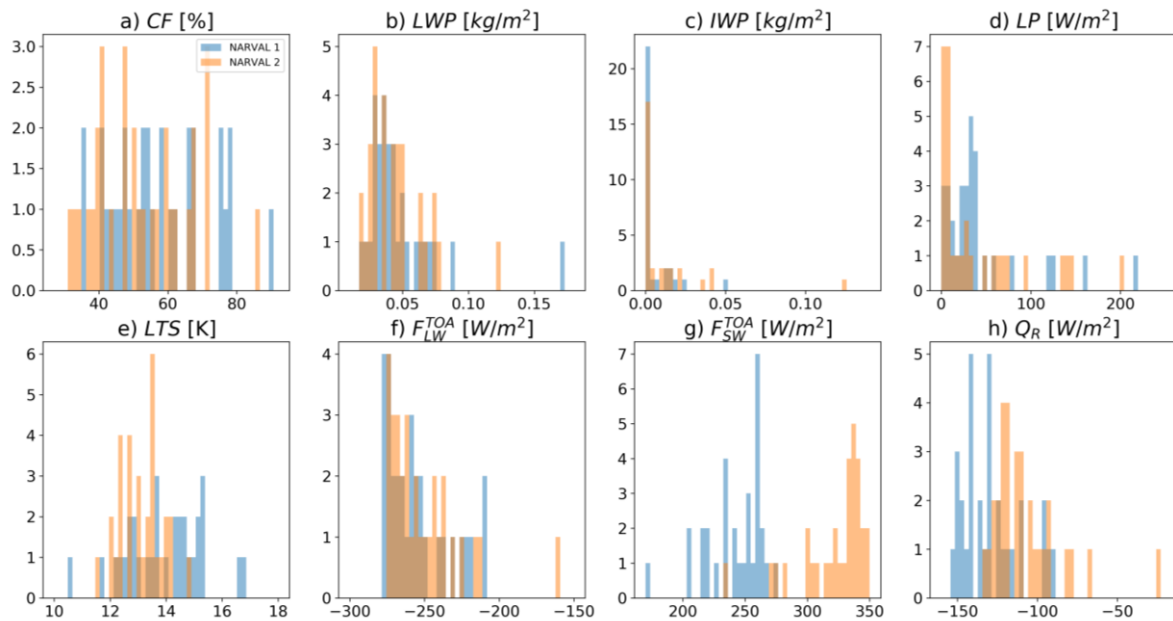
147

148 **Results**

149 Conducting daily simulations over two months at different seasons allows us to sample a large
150 ensemble of initial conditions and cloud types (see Fig. 2 and Table 1). To identify statistically

151 significant differences between the two months, we conduct independent t-test (p-values are
 152 presented in Table 1). This demonstrates that the lower tropospheric stability (LTS), top of
 153 atmosphere shortwave flux (F_{SW}^{TOA}), and the atmospheric column radiative term (Q_R) are different
 154 in a statistically significant manner (p-value < 0.05) between the two different months. The
 155 differences in other parameters (cloud fraction – CF, liquid water path - LWP, ice water path –
 156 IWP, latent heat of precipitation – LP, and top of atmosphere longwave flux - F_{LW}^{TOA}) are not
 157 statistically significant (Table 1).

158
 159



160
 161 **Figure 2. Histograms of mean (time and space) cloud and atmospheric properties for the base simulations**
 162 **with $CDNC = 20 \text{ cm}^{-3}$ (clean simulations) for each day of the two months that were simulated. Blue**
 163 **represents the NARVAL 1 month (December 2013), while orange the NARVAL 2 month (August 2016). a)**
 164 **cloud fraction – CF, b) liquid water path - LWP, c) ice water path – IWP, d) precipitation latent heat flux**
 165 **- LP, e) lower tropospheric stability – LTS, f) top of atmosphere longwave flux - F_{LW}^{TOA} , g) top of atmosphere**
 166 **shortwave flux - F_{SW}^{TOA} , and h) atmospheric column radiative term - Q_R .**

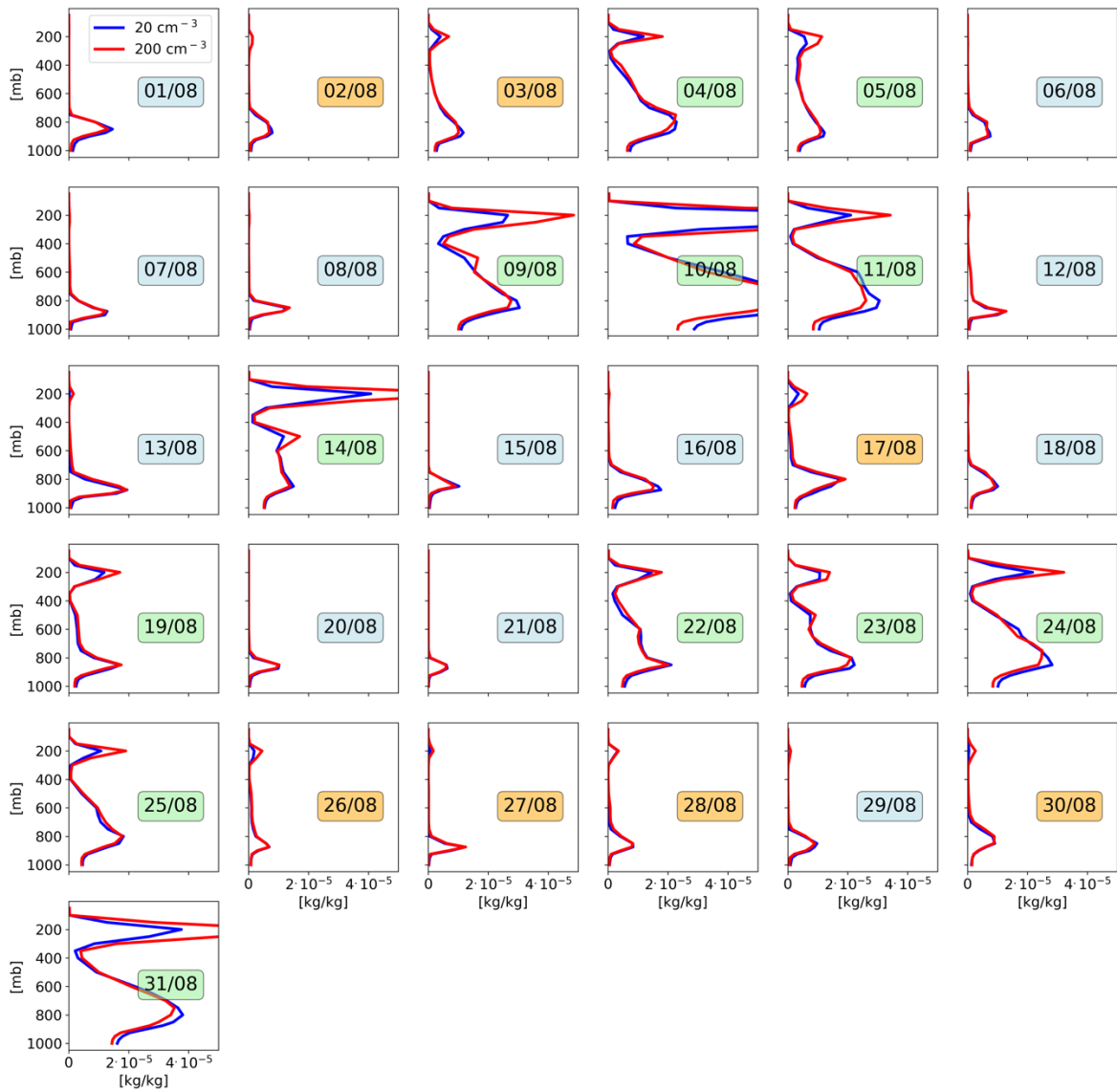
167
 168
 169
 170
 171
 172
 173
 174
 175
 176

177 **Table 1. The monthly mean value of each of the properties presented in Fig. 2 \pm 1 standard deviation for**
 178 **each month and the p-value of the two-sample independent t-test. The p-values which demonstrate a**
 179 **significant difference between the months (<0.05) are presented in bold.**

	Mean NARVAL 1	Mean NARVAL 2	p-value t-test
CF [%]	57.2 ± 13.7	52.3 ± 13.4	0.16
LWP [kg/m^2]	$4.8 \cdot 10^{-2} \pm 2.8 \cdot 10^{-2}$	$4.5 \cdot 10^{-2} \pm 2.2 \cdot 10^{-2}$	0.66
IWP [kg/m^2]	$5.7 \cdot 10^{-3} \pm 1.1 \cdot 10^{-2}$	$1.2 \cdot 10^{-2} \pm 2.4 \cdot 10^{-2}$	0.19
LP [W/m^2]	43.8 ± 47.8	52.2 ± 78.2	0.6
LTS [K]	13.9 ± 1.4	13.1 ± 0.7	$7 \cdot 10^{-3}$
F_{LW}^{TOA} [W/m^2]	-254.2 ± 21.2	-251.7 ± 23.5	0.66
F_{SW}^{TOA} [W/m^2]	241.7 ± 22.5	321.9 ± 26.4	$1.4 \cdot 10^{-18}$
Q_R [W/m^2]	-129.2 ± 17.8	-107.8 ± 21.7	$9.8 \cdot 10^{-5}$

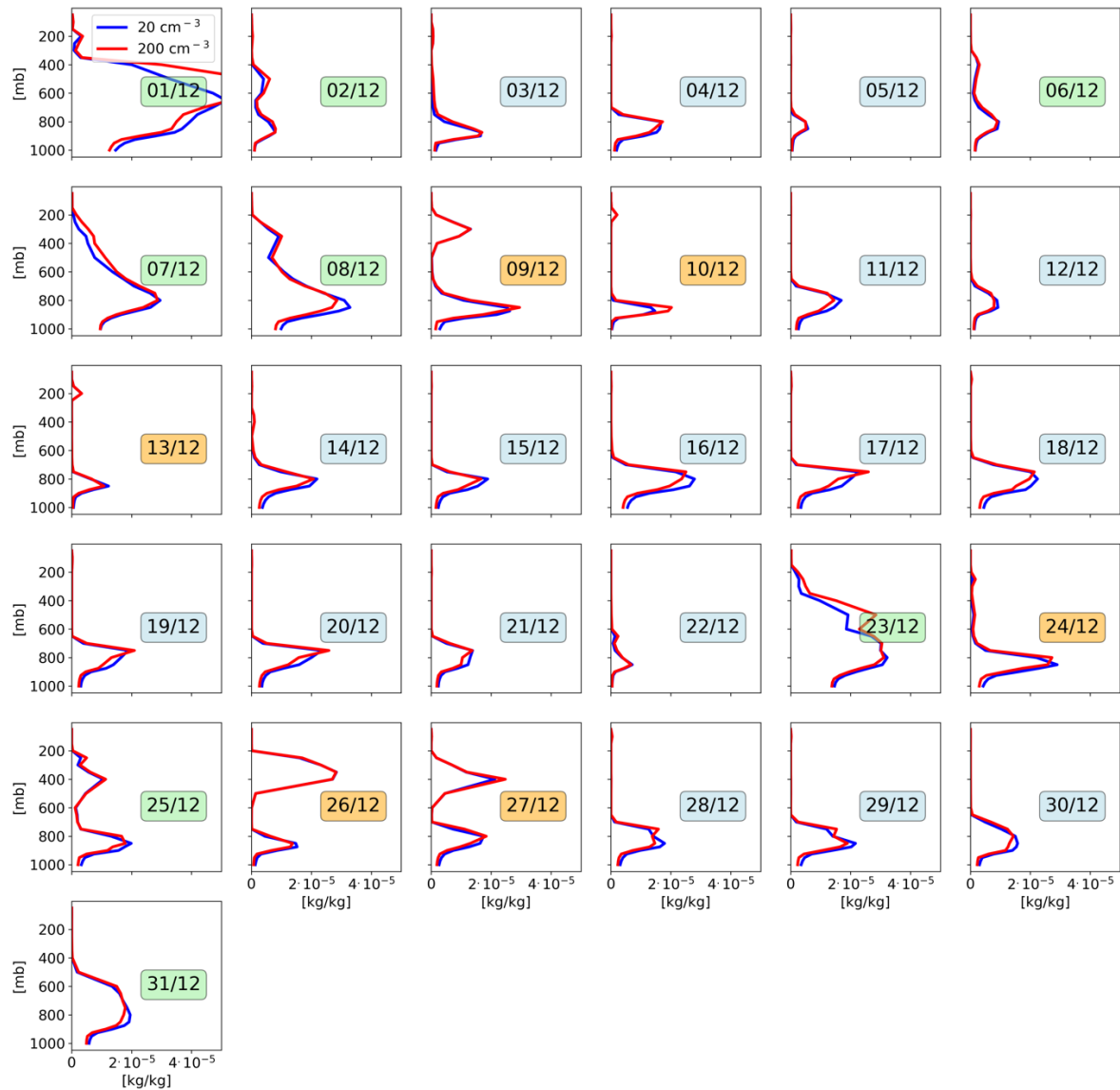
180
 181
 182
 183
 184
 185
 186
 187
 188
 189
 190
 191
 192

Figures 3 and 4 present vertical profiles of the total water (liquid and ice) mixing ratio from the different simulations during NARVAL 2 (August 2016) and NARVAL 1 (December 2013), respectively. Generally, during the winter month (NARVAL 1) the clouds are shallower than in the summer month (NARVAL 2), although there is significant variability. This is expected due to the seasonality of the ITCZ location (Stevens et al., 2016). The simulated days are manually separated to three different cloud regimes based on the domain and time mean total water mixing ratio vertical profiles. The cloud regimes considered here are: shallow clouds (shallow-cloud dominated days), two-layer clouds (shallow cloud layer and a cirrus cloud layer) and deep clouds (deep-cloud dominated days).



193
 194 **Figure 3. Mean (time and space) vertical profiles of the total water (liquid and ice) mixing ratio in each**
 195 **simulation (each last for 24 hours) for the NARVAL 2 month (August 2016). Blue: clean conditions (20 cm^{-3}**
 196 **3), red: polluted conditions (200 cm^{-3}). The simulated days are separated into three different cloud regimes:**
 197 **shallow clouds (blue date box), two-layer clouds (shallow cloud layer and a cirrus cloud layer – orange date**
 198 **box) and deep clouds (green date box).**

199
 200



201
 202 **Figure 4. Same as Fig. 3 but for the NARVAL 1 month (December 2013).**

203
 204 Figure 5 presents histograms of aerosol effects (polluted minus clean) for the different
 205 simulations. The distribution of changes in cloud fraction (Fig. 5a) demonstrate small mean
 206 values for both months (-0.3% and 0.1% for the winter and summer month, respectively) which
 207 is slightly more skewed to positive values in the summer. Examining the significance of these
 208 trends with a t-test demonstrates that only the winter month response is statistically significant
 209 (Table 2). The CDNC effect on the liquid water path (LWP; Fig. 5b) and the ice water path
 210 (IWP; Fig. 5c) is shown to be almost entirely positive (or zero) in both months and differs from
 211 zero in a statistically significant manner. The mean change in precipitation (Fig. 5d) is small
 212 and negative (slightly more negative during the winter month). However, during the summer
 213 month it is not statistically significant and can be either positive or negative. We note that the

214 mean precipitation decreases during the winter month (which is statistically significant) is
215 small and equivalent to 0.07 mm/day (-1.8 W/m²). Increasing CDNC systematically decreases
216 LTS (Fig. 5e), representing deepening of the boundary layer (Dagan et al., 2016;Lebo and
217 Morrison, 2014;Seifert et al., 2015;Stevens and Feingold, 2009). This trend is statistically
218 significant for both months (Table 2).

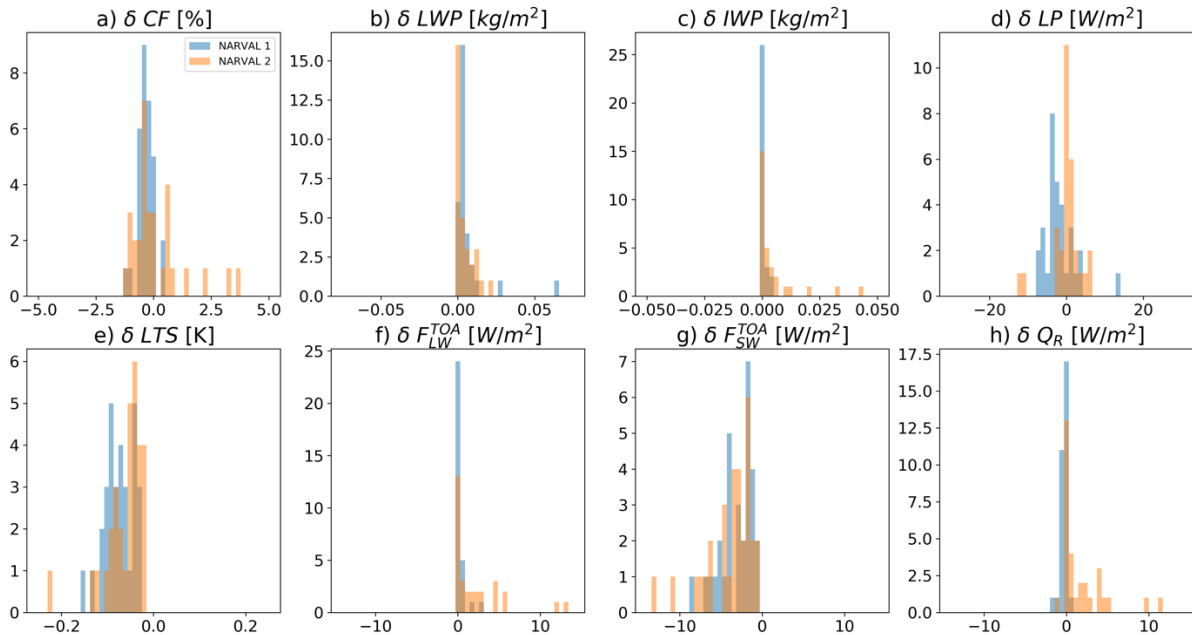
219 The CDNC effect on F_{LW}^{TOA} is positive and small (average of 0.24 W/m²) in the winter month
220 (but still statistically significant) and larger (average of 2.16 W/m²) in the summer month (Fig.
221 5f – positive flux downwards), primarily due to an increase in ice water content under polluted
222 conditions (see also Figs. 3, 4 and 5c). We previously showed that an increase in CDNC drives
223 an increase in the ice content at the upper troposphere and hence a reduction in the outgoing
224 LW radiation (Dagan et al., 2019); here we show that this trend is statistically significant (Fig.
225 5c). However, during the winter, when deep convective clouds are less abundant and the
226 atmosphere is more stable, the LW flux is less affected.

227 The CDNC effect on F_{SW}^{TOA} is always negative (Fig. 5g) and is on average -3.6 W/m² and -3.8
228 W/m² in the winter and summer month, respectively (the difference between the two months
229 is not statistically significant; however, both differ from zero in a statistically significant
230 manner -Table 2). The negative F_{SW}^{TOA} effect is caused mostly due to the Twomey effect
231 (Twomey, 1977) and the LWP/IWP effect (Albrecht, 1989;Koren et al., 2010;Malavelle et al.,
232 2017) (Figs. 5b and 5c), as the CF changes are small (Fig. 5a). For exploring the relative role
233 of the Twomey and IWP/LWP effects, we ran all simulations again with the Twomey effect
234 turned off. Without the Twomey effect the SW effect is reduced by up to a factor of 10 (-0.35
235 W/m² compared with -3.6 W/m² in the winter month, and -1.0 W/m² compared with -3.8 W/m²
236 in the summer month). This demonstrates that the Twomey effect is the dominant factor
237 underlying the F_{SW}^{TOA} changes. Radiative effects due to changes in ice size distribution are not
238 considered due to uncertainties in the evolution of ice morphology. Accounting for this effect
239 would likely further increase the relative role of the Twomey effect compared to the cloud
240 adjustment effects (CF and LWP/IWP adjustments).

241 The change in the atmospheric column radiative warming term Q_R is shown to be small for the
242 winter month (-0.26 W/m² on average) but much larger and positive for the summer month
243 (1.8 W/m² on average). The increase in Q_R during the summer is caused due to the effect of
244 deep, ice containing clouds on the outgoing LW flux (Fig. 5f). SW flux changes due to CDNC
245 perturbations (Fig. 5g) have a much smaller effect on Q_R as the SW absorption of clouds is
246 small (Dagan et al., 2019).

247 Examining the similarity between the response of the different properties to the CDNC
 248 perturbation in the two different months (Table 2) reveals that the responses of the IWP, F_{LW}^{TOA} ,
 249 Q_R and F_{SW+LW}^{TOA} (the net TOA LW and SW effects – Fig. 10 below) are different in a statistically
 250 significant manner between the two months. As will be shown below, this is related to the
 251 response of the ice content.

252
 253



254
 255 **Figure 5. Histograms of the domain and time mean response of cloud and atmospheric properties to CDNC**
 256 **perturbation (polluted simulations minus clean simulations) for each day of the two months that were**
 257 **simulated. Blue represents the NARVAL 1 month (December 2013), while orange the NARVAL 2 month**
 258 **(August 2016). a) cloud fraction – CF, b) liquid water path - LWP, c) ice water path – IWP, d) precipitation**
 259 **latent heat flux - LP, e) lower tropospheric stability – LTS, f) top of atmosphere longwave flux - F_{LW}^{TOA} , g)**
 260 **top of atmosphere shortwave flux - F_{SW}^{TOA} , and h) atmospheric column radiative term - Q_R .**

261
 262
 263
 264
 265
 266
 267
 268
 269
 270

271 **Table 2. Summary of monthly mean response of cloud and atmospheric properties (presented in Fig. 5) to**
 272 **the CDNC perturbation (polluted simulations minus clean simulations) ± 1 standard deviation for each**
 273 **month. In addition, the p-values of the two-sample independent t-test are presented, as well as the p-values**
 274 **for comparing the CDNC response in each month to zero. The p-values which demonstrate significant**
 275 **difference (<0.05) are presented in bold.**

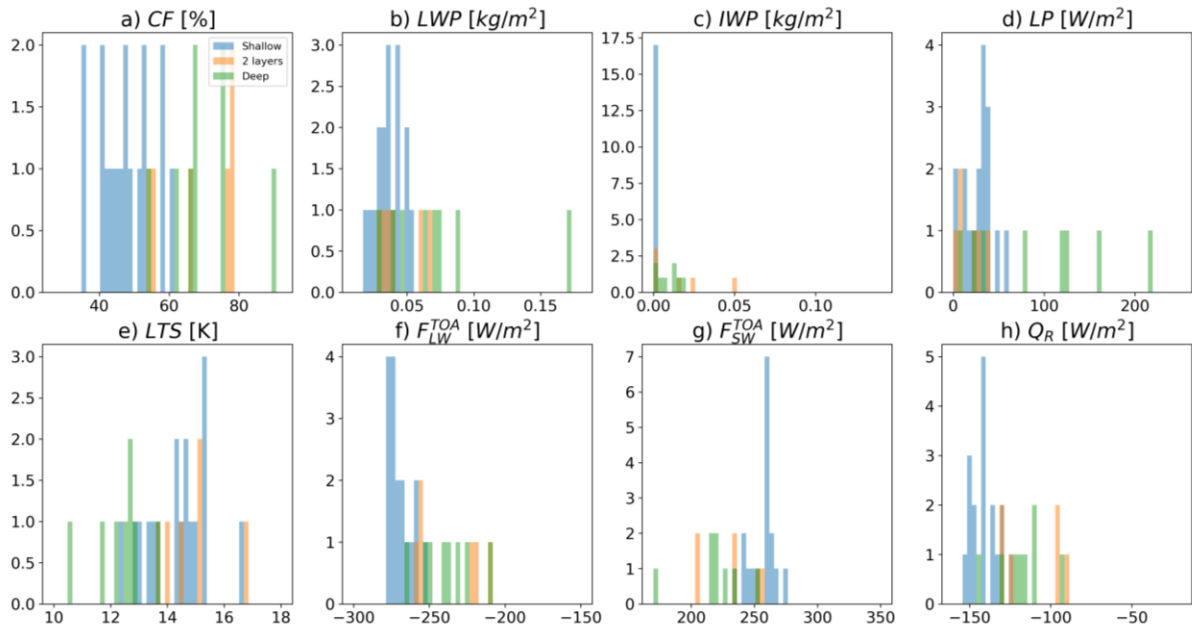
	Mean NARVAL 1	Mean NARVAL 2	p-value t-test	p-value one sample t- test compare to 0 - NARVAL 1	p-value one sample t- test compare to 0 - NARVAL 2
δCF [%]	-0.32 ± 0.31	0.11 ± 1.15	0.053	$8.1 \cdot 10^{-6}$	0.6
δLWP [kg/m^2]	$6.5 \cdot 10^{-3} \pm 1.2 \cdot 10^{-2}$	$4.0 \cdot 10^{-3} \pm 5.4 \cdot 10^{-3}$	0.3	$4.4 \cdot 10^{-3}$	$3.5 \cdot 10^{-4}$
δIWP [kg/m^2]	$5.6 \cdot 10^{-4} \pm 1.3 \cdot 10^{-3}$	$8.2 \cdot 10^{-3} \pm 1.9 \cdot 10^{-2}$	0.035	0.02	0.03
δLP [W/m^2]	-1.8 ± 4.1	-1.2 ± 7.0	0.7	0.02	0.37
δLTS [K]	-0.075 ± 0.031	-0.062 ± 0.042	0.18	$3.2 \cdot 10^{-14}$	$4.3 \cdot 10^{-9}$
δF_{LW}^{TOA} [W/m^2]	0.24 ± 0.60	2.16 ± 3.25	0.002	0.03	0.001
δF_{SW}^{TOA} [W/m^2]	-3.6 ± 3.5	-3.8 ± 2.9	0.8	$3.3 \cdot 10^{-6}$	$4.7 \cdot 10^{-8}$
δQ_R [W/m^2]	-0.26 ± 0.39	1.8 ± 2.8	$1.8 \cdot 10^{-4}$	$9.7 \cdot 10^{-4}$	$1.4 \cdot 10^{-3}$
δF_{SW+LW}^{TOA}	-3.36 ± 3.02	-1.67 ± 1.93	0.01	$1.1 \cdot 10^{-6}$	$5.1 \cdot 10^{-5}$

276

277 CDNC effect on different cloud regimes

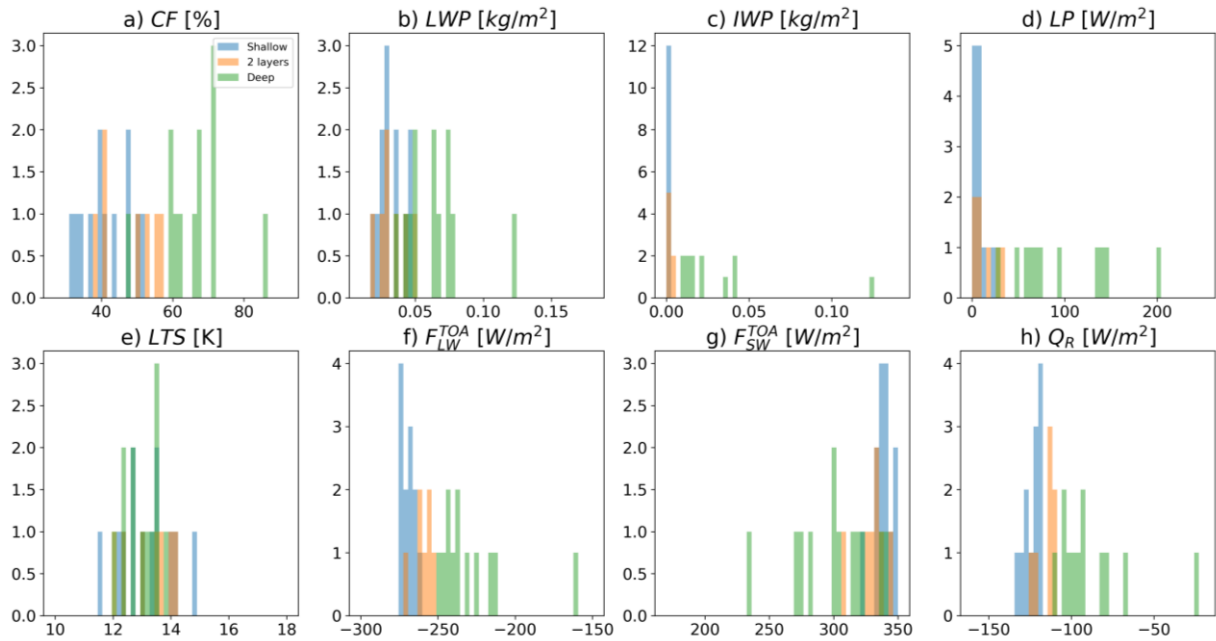
278 For better understanding the trend demonstrated in Fig. 5 and Table 2, we split the simulated
 279 days into different dominant cloud types/regimes (see Figs. 3 and 4). Figures 6 and 7 present
 280 histograms of the same atmospheric properties presented in Fig. 2 but separated by different
 281 cloud regimes – shallow clouds, two-layer clouds (shallow clouds with cirrus cloud layer
 282 above), and deep clouds. These figures demonstrate that the cloud fraction, LWP, IWP,
 283 precipitation, F_{LW}^{TOA} and Q_R are generally higher on days dominated by deep-clouds as compared
 284 to days dominated by shallow clouds, while the LTS and F_{SW}^{TOA} are lower in the deep-cloud
 285 dominated days compared to shallow-cloud dominated days (with the two-layer cloud days
 286 generally in-between them). The separation into different cloud regimes also demonstrates that
 287 more deep-cloud days are occurring during the summer month as compared to the winter month
 288 (12 compare to 8) and that the deep clouds during summer are deeper and contain more water.
 289 The larger occurrence of deep convection during the summer month is consistent with the
 290 statistically significant reduction in LTS (Fig. 2 and Table 1) and is expected based on the local
 291 seasonality (Stevens et al., 2016).

292



293
 294
 295
 296
 297
 298
 299
 300
 301
 302

Figure 6. Histograms of mean (time and space) cloud and atmospheric properties for the base simulations with $CDNC = 20 \text{ cm}^{-3}$ (clean simulations) for each day of the NARVAL 1 month (December 2013) separated into different cloud regimes: shallow clouds (blue), two-layer clouds (shallow clouds with cirrus clouds layer above - orange), and deep clouds (green). a) cloud fraction – CF, b) liquid water path - LWP, c) ice water path – IWP, d) precipitation latent heat flux - LP, e) lower tropospheric stability – LTS, f) top of atmosphere longwave flux - F_{LW}^{TOA} , g) top of atmosphere shortwave flux - F_{SW}^{TOA} , and h) atmospheric column radiative term - Q_R .

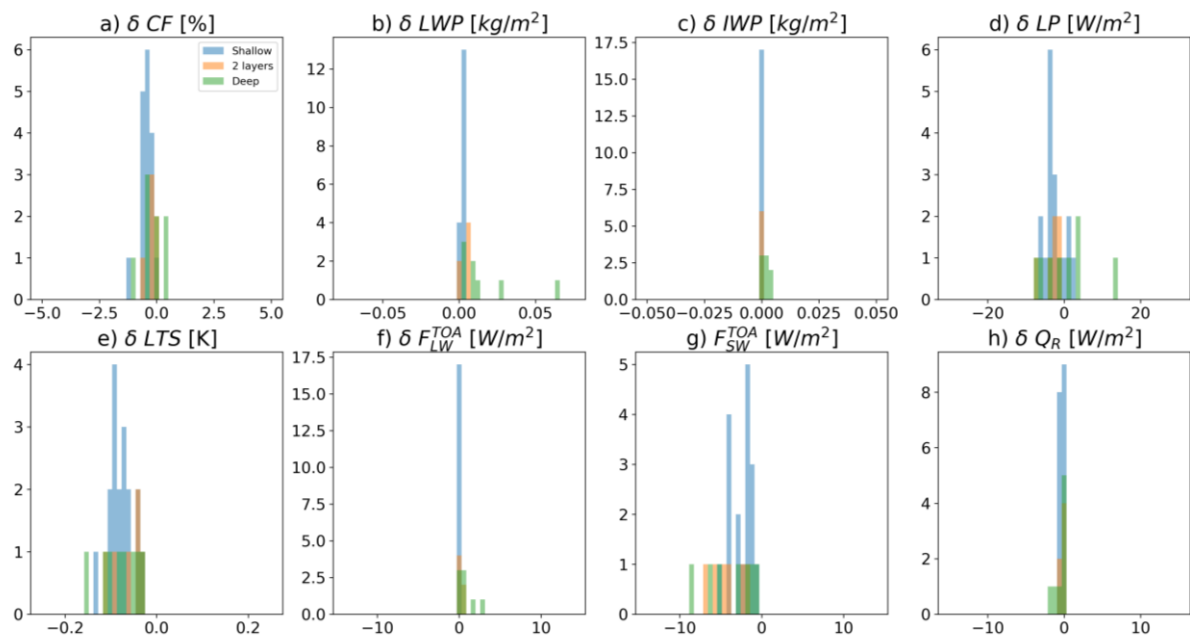


303
 304
 305
 306

Figure 7. Same as Fig. 6 but for the NARVAL 2 month (August 2016).

307 Examining the response of the different cloud regimes to the CDNC perturbation (Figs. 8 and
 308 9) demonstrates that the response of the cloud fraction, LWP, IWP and F_{LW}^{TOA} in the deep-cloud
 309 days is generally more positive, while the response of F_{LW}^{TOA} and LTS is generally more negative.
 310 These trends are more pronounced during the summer month as compared to the winter month.
 311 The response of Q_R is more positive in the deep-cloud dominated days in the summer month
 312 but does not show any different trend in the winter month. The precipitation response does not
 313 show any distinct different trend for the different cloud types in both months.
 314 The findings presented in Figs. 8 and 9 demonstrate that the IWP response in the deep-cloud
 315 dominated days is generally stronger in the summer month as compare to the winter month.
 316 The increase in the IWP with the increase in CDNC drives a reduction in F_{LW}^{TOA} and hence
 317 increase in Q_R (Dagan et al., 2019). We note that the largest difference between the two months
 318 emerges due to the stronger response of the ice content in the summer month as compared to
 319 the winter month. This fact can explain the statistically significant different response of the
 320 IWP, F_{LW}^{TOA} and Q_R shown in Table 2.

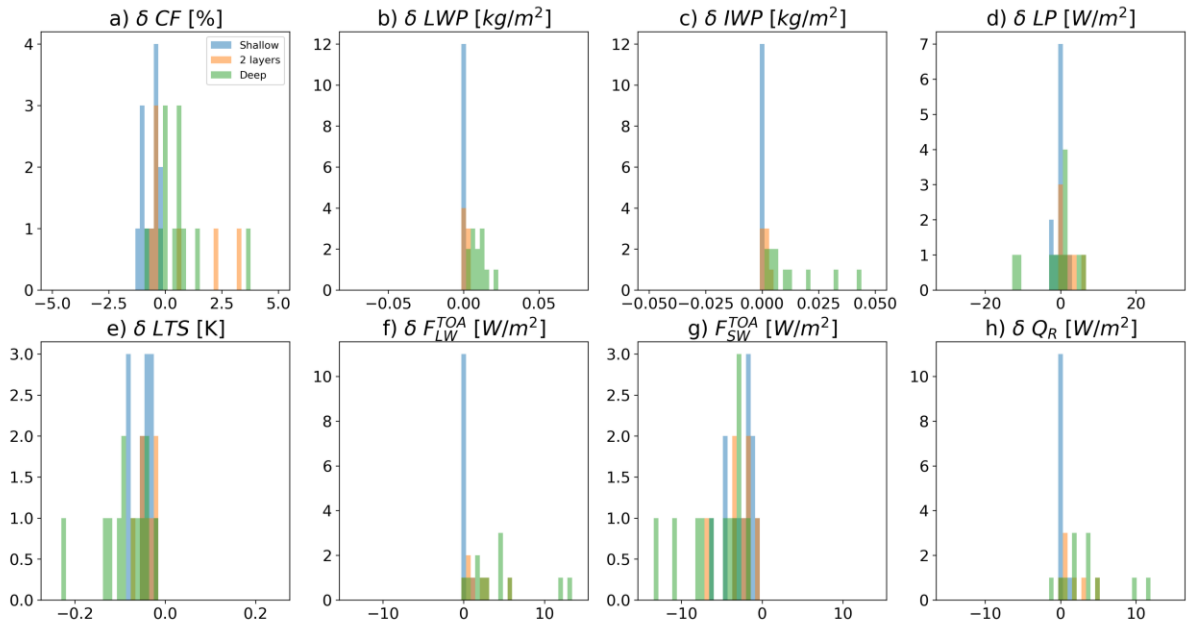
321
 322
 323



324

325 **Figure 8. Histograms of the domain and time mean response of cloud and atmospheric properties to the**
 326 **CDNC perturbation (polluted simulations minus clean simulations) for each day of the NARVAL 1 month**
 327 **(December 2013) separated into the different cloud regimes: shallow clouds (blue), two-layer clouds**
 328 **(shallow clouds with cirrus clouds layer above - orange), and deep clouds (green). a) cloud fraction – CF,**
 329 **b) liquid water path - LWP, c) ice water path – IWP, d) precipitation latent heat flux - LP, e) lower**

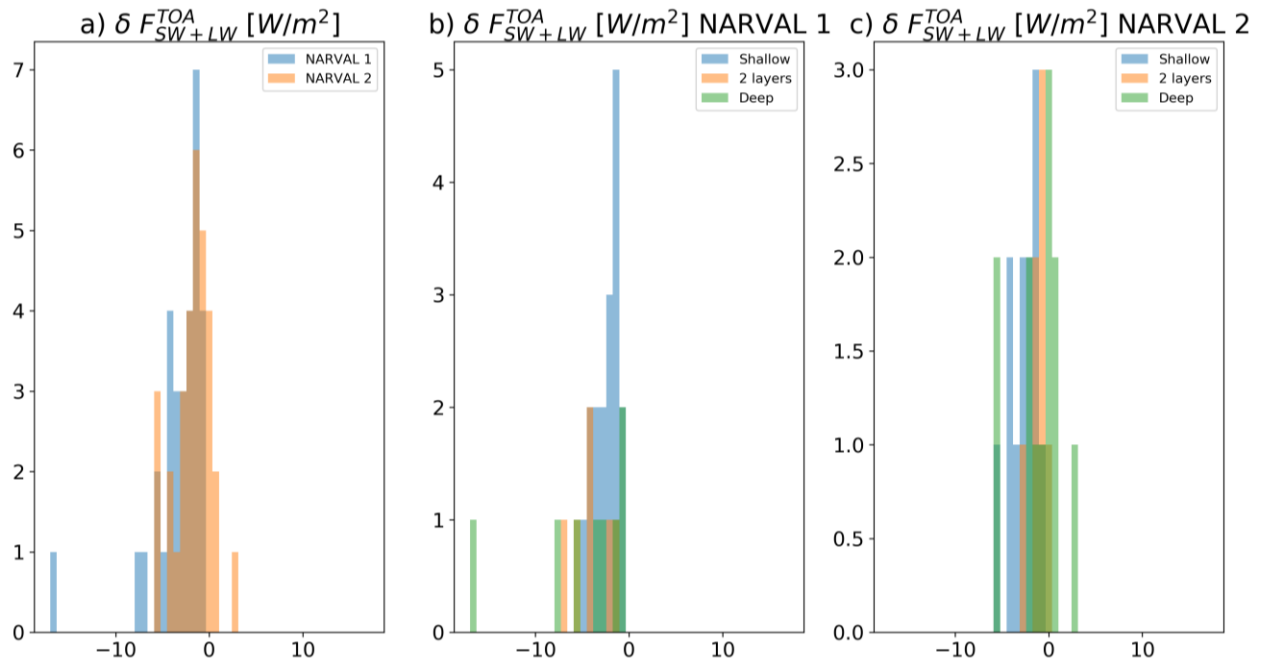
330 tropospheric stability – LTS, f) top of atmosphere longwave flux - F_{LW}^{TOA} , g) top of atmosphere shortwave
 331 flux - F_{SW}^{TOA} , and h) atmospheric column radiative term - Q_R .
 332
 333



334
 335 **Figure 9.** Same as Fig. 8 but for the NARVAL 2 month (August 2016).
 336

337 The combined CDNC effect on the total net TOA radiation (F_{SW+LW}^{TOA}) is shown in Fig. 10. It
 338 demonstrates that during the winter month the effect on F_{SW+LW}^{TOA} is always negative and has a
 339 mean value of -3.4 W/m^2 . However, during the summer month, the mean effect is less negative
 340 (-1.7 W/m^2) and for some of the days it could even be positive due to the effect of the CDNC
 341 on the ice water content (Fig. 5 and Table 2). The difference between the two months in F_{SW+LW}^{TOA}
 342 is statistically significant (Table 2). We note that during the summer month all days for which
 343 $F_{SW+LW}^{TOA} \geq 0$ are deep-cloud dominated days, supporting the hypothesis that the difference
 344 between the different months are driven by the different response of the deep clouds, which are
 345 deeper and contain more water in the summer month.

346



347
 348 **Figure 10. Histograms of the response of the net (shortwave + longwave) top of atmosphere radiative flux**
 349 **(F_{SW+LW}^{TOA}) to the CDNC perturbation (polluted simulations minus clean simulations) for each of the**
 350 **simulated days. In a) blue represents the NARVAL 1 month (December 2013), while orange the NARVAL**
 351 **2 month (August 2016). In b) and c) the NARVAL 1 and the NARVAL 2 months are separated to the**
 352 **different cloud regimes: shallow clouds (blue), two-layer clouds (shallow clouds with cirrus clouds layer**
 353 **above - orange), and deep clouds (green).**

354
 355
 356
 357

Summary and Conclusions

358 Ensemble daily simulations over a region near Barbados for two separate month-long periods
 359 were conducted to investigate aerosol effects on cloud properties and the atmospheric energy
 360 budget. For each day, two simulations were conducted with low and high CDNC representing
 361 clean and polluted conditions, respectively. These simulations are used to distinguish between
 362 properties that are robustly affected by changes in CDNC and those that are not. For example,
 363 we have shown that, for the entire set of simulations (62 different days), an increase in CDNC
 364 always drives a reduction in the lower tropospheric stability (Fig. 5). In addition, F_{SW}^{TOA} is always
 365 reduced by an increase in CDNC, representing more SW reflection. However, changes in cloud
 366 fraction or precipitation are not as robust, and, despite the fact that for a given day they could
 367 be large, they are on average not distinguishable from zero (at least for the summer month).
 368 However, we note that the aerosol response we present here may be underestimated due to the
 369 effect of the fixed boundary conditions. In addition, using a microphysical scheme that assumes
 370 saturation adjustment reduces the sensitivity of the clouds to aerosol perturbation (Koren et al.,
 371 2014; Dagan et al., 2015a; Heiblum et al., 2016; Fan et al., 2018). However, this might be a

372 small effect in our case as the phase change relaxation time of condensation and evaporation is
373 usually on the order of a few seconds (Pinsky et al., 2013). Hence, even if we would use a
374 microphysical scheme that explicitly resolves condensation and evaporation, the humidity is
375 expected to get back to saturation on shorter time scales than the temporal resolution of the
376 model (12 sec), and hence, practically we will be in “saturation adjustment” conditions anyway.
377 We also note that using 1200 m horizontal resolution does not properly resolve all shallow
378 cumulus clouds (Naumann and Kiemle, 2019).

379 The use of two month-long periods, covering different seasons dominated by different
380 meteorological conditions and cloud type, demonstrate again (Altaratz et al., 2014; Lee et al.,
381 2009; Mülmenstädt and Feingold, 2018; van den Heever et al., 2011; Rosenfeld et al.,
382 2013; Glassmeier and Lohmann, 2016; Gryspeerdt and Stier, 2012; Dagan et al., 2015a), that the
383 aerosol effect on clouds is strongly dependent on cloud regimes and meteorological conditions.
384 For our simulations we demonstrate that the top of atmosphere net radiative effect in this region
385 is twice as large during the winter month as compared to the summer month (Fig. 10).

386 To better understand these differences we have split the simulated days into three different
387 dominant cloud regimes. The results demonstrate that most of the differences in the response
388 to CDNC increases between the two months are driven by the response of the ice content in
389 deep convective clouds. During the summer month, the atmosphere is less stable and the deep
390 convective clouds in the base-line simulations are more abundant, reach higher levels in the
391 atmosphere and contain more water. These more developed clouds respond stronger to the
392 CDNC perturbations and develop more ice content than the shallower clouds during the winter
393 month. The increased ice is driven by increase in mass flux to the upper levels. The added ice
394 content reduces the outgoing LW flux at the TOA and hence compensates some of the SW
395 effect, which itself is similar between the summer and winter months.

396 Our results highlight the need to use large ensembles of initial conditions for cloud-aerosol
397 interaction studies, even in large domain simulations, and suggest that caution is needed when
398 trying to draw conclusions from a single case-study experiments and short-term observations.

399

400 **Author contributions.** G. D. carried out the simulations and analyses presented. P. S. assisted
401 with the design and interpretation of the analyses. G.D. prepared the manuscript with
402 contributions from P.S.

403

404

405

406 **Acknowledgements:**

407 This research was supported by the European Research Council (ERC) project constRaining
408 the EffeCts of Aerosols on Precipitation (RECAP) under the European Union's Horizon 2020
409 research and innovation programme with grant agreement No 724602. The simulations were
410 performed using the ARCHER UK National Supercomputing Service. We acknowledge MPI,
411 DWD and DKRZ for the NARVAL simulations.

412

413 **References**

414 Albrecht, B. A.: Aerosols, cloud microphysics, and fractional cloudiness, *Science* (New York,
415 NY), 245, 1227, 1989.

416 Altaratz, O., Koren, I., Remer, L., and Hirsch, E.: Review: Cloud invigoration by aerosols—
417 Coupling between microphysics and dynamics, *Atmospheric Research*, 140, 38-60, 2014.

418 Bellouin, N., Quaas, J., Gryspeerdt, E., Kinne, S., Stier, P., Watson-Parris, D., Boucher, O.,
419 Carslaw, K., Christensen, M., and Daniau, A.-L.: Bounding aerosol radiative forcing of climate
420 change, *Reviews of Geophysics*, 2019.

421 Boucher, O., Randall, D., Artaxo, P., Bretherton, C., Feingold, G., Forster, P., Kerminen, V.,
422 Kondo, Y., Liao, H., and Lohmann, U.: Clouds and aerosols, *Climate Change*, 571-657, 2013.

423 Chen, Q., Koren, I., Altaratz, O., Heiblum, R. H., Dagan, G., and Pinto, L.: How do changes
424 in warm-phase microphysics affect deep convective clouds?, *Atmospheric Chemistry and*
425 *Physics*, 17, 9585-9598, 2017.

426 Christensen, M. W., Chen, Y. C., and Stephens, G. L.: Aerosol indirect effect dictated by liquid
427 clouds, *Journal of Geophysical Research: Atmospheres*, 121, 2016.

428 Clough, S., Shephard, M., Mlawer, E., Delamere, J., Iacono, M., Cady-Pereira, K., Boukabara,
429 S., and Brown, P.: Atmospheric radiative transfer modeling: a summary of the AER codes,
430 *Journal of Quantitative Spectroscopy and Radiative Transfer*, 91, 233-244, 2005.

431 Dagan, G., Koren, I., and Altaratz, O.: Competition between core and periphery-based
432 processes in warm convective clouds—from invigoration to suppression, *Atmospheric*
433 *Chemistry and Physics*, 15, 2749-2760, 2015a.

434 Dagan, G., Koren, I., and Altaratz, O.: Aerosol effects on the timing of warm rain processes,
435 *Geophysical Research Letters*, 42, 4590-4598, 10.1002/2015GL063839, 2015b.

436 Dagan, G., Koren, I., Altaratz, O., and Heiblum, R. H.: Aerosol effect on the evolution of the
437 thermodynamic properties of warm convective cloud fields, *Scientific Reports*, 38769,
438 <https://doi.org/10.1038/srep38769>, 2016.

439 Dagan, G., Koren, I., Altaratz, O., and Heiblum, R. H.: Time-dependent, non-monotonic
440 response of warm convective cloud fields to changes in aerosol loading, *Atmos. Chem. Phys.*,
441 17, 7435-7444, 10.5194/acp-17-7435-2017, 2017.

442 Dagan, G., Koren, I., and Altaratz, O.: Quantifying the effect of aerosol on vertical velocity
443 and effective terminal velocity in warm convective clouds, *Atmospheric Chemistry and*
444 *Physics*, 18, 6761-6769, 2018a.

445 Dagan, G., Koren, I., Kostinski, A., and Altaratz, O.: Organization and oscillations in simulated
446 shallow convective clouds, *Journal of Advances in Modeling Earth Systems*, 2018b.

447 Dagan, G., Stier, P., Christensen, M., Cioni, G., Klocke, D., and Seifert, A.: Atmospheric
448 energy budget response to idealized aerosol perturbation in tropical cloud systems, *Atmos.*
449 *Chem. Phys. Discuss.*, <https://doi.org/10.5194/acp-2019-813>, in press, 2019.

450 Heiblum, R.H., Altaratz, O., Koren, I., Feingold, G., Kostinski, A.B., Khain, A.P.,
451 Ovchinnikov, M., Fredj, E., Dagan, G., Pinto, L. and Yaish, R.: Characterization of cumulus
452 cloud fields using trajectories in the center of gravity versus water mass phase space: 2. Aerosol
453 effects on warm convective clouds. *Journal of Geophysical Research: Atmospheres*, 121(11),
454 pp.6356-6373, 2016.

455 Fan, J., Zhang, R., Li, G., and Tao, W.-K.: Effects of aerosols and relative humidity on cumulus
456 clouds, *Journal of Geophysical Research-Atmospheres*, 112, 10.1029/2006jd008136, 2007.

457 Fan, J., Yuan, T., Comstock, J. M., Ghan, S., Khain, A., Leung, L. R., Li, Z., Martins, V. J.,
458 and Ovchinnikov, M.: Dominant role by vertical wind shear in regulating aerosol effects on
459 deep convective clouds, *Journal of Geophysical Research-Atmospheres*, 114,
460 10.1029/2009jd012352, 2009.

461 Fan, J., D. Rosenfeld, Y. Ding, L. R. Leung, and Z. Li.: Potential aerosol indirect effects on
462 atmospheric circulation and radiative forcing through deep convection. *Geophys. Res. Lett.*,
463 doi:10.1029/2012GL051851, 2012.

464 Fan, J., Rosenfeld, D., Zhang, Y., Giangrande, S.E., Li, Z., Machado, L.A., Martin, S.T., Yang,
465 Y., Wang, J., Artaxo, P. and Barbosa, H.M.: Substantial convection and precipitation
466 enhancements by ultrafine aerosol particles. *Science*, 359(6374), pp.411-418, 2018.

467 Glassmeier, F., and Lohmann, U.: Constraining precipitation susceptibility of warm-, ice-, and
468 mixed-phase clouds with microphysical equations, *Journal of the Atmospheric Sciences*, 73,
469 5003-5023, 2016.

470 Grabowski, W. W.: Untangling microphysical impacts on deep convection applying a novel
471 modeling methodology, *Journal of the Atmospheric Sciences*, 72, 2446-2464, 2015.

472 Gryspeerd, E., and Stier, P.: Regime-based analysis of aerosol-cloud interactions, *Geophysical*
473 *Research Letters*, 39, 2012.

474 Gryspeerd, E., Goren, T., Sourdeval, O., Quaas, J., Mülmenstädt, J., Dipu, S., Unglaub, C.,
475 Gettelman, A., and Christensen, M.: Constraining the aerosol influence on cloud liquid water
476 path, *Atmospheric Chemistry and Physics*, 19, 5331-5347, 2019.

477 Gustafson Jr, W., and Vogelmann, A.: LES ARM Symbiotic Simulation and Observation
478 (LASSO) Implementation Strategy, DOE Office of Science Atmospheric Radiation
479 Measurement (ARM) Program , 2015.

480 Gustafson, W. I., Vogelmann, A. M., Cheng, X., Endo, S., Krishna, B., Li, Z., Toto, T., and
481 Xiao, H.: Description of the LASSO Alpha 2 Release, DOE Office of Science Atmospheric
482 Radiation Measurement (ARM) Program , 2017.

483 Heikenfeld, M., White, B., Labbouz, L., and Stier, P.: Aerosol effects on deep convection: the
484 propagation of aerosol perturbations through convective cloud microphysics, *Atmospheric*
485 *Chemistry and Physics*, 19, 2601-2627, 2019.

486 Iacono, M. J., Delamere, J. S., Mlawer, E. J., Shephard, M. W., Clough, S. A., and Collins, W.
487 D.: Radiative forcing by long-lived greenhouse gases: Calculations with the AER radiative
488 transfer models, *Journal of Geophysical Research: Atmospheres*, 113, 2008.

489 Kalina, E. A., Friedrich, K., Morrison, H., and Bryan, G. H.: Aerosol effects on idealized
490 supercell thunderstorms in different environments, *Journal of the Atmospheric Sciences*, 71,
491 4558-4580, 2014.

492 Khain, A., Rosenfeld, D., and Pokrovsky, A.: Aerosol impact on the dynamics and
493 microphysics of deep convective clouds, *Quarterly Journal of the Royal Meteorological*
494 *Society*, 131, 2639-2663, 10.1256/qj.04.62, 2005.

495 Khain, A. P., BenMoshe, N., and Pokrovsky, A.: Factors determining the impact of aerosols
496 on surface precipitation from clouds: An attempt at classification, *Journal of the Atmospheric*
497 *Sciences*, 65, 1721-1748, 10.1175/2007jas2515.1, 2008.

498 Klepp, C., Ament, F., Bakan, S., Hirsch, L., and Stevens, B.: The NARVAL Campaign Report,
499 2014.

500 Klocke, D., Brueck, M., Hohenegger, C., and Stevens, B.: Rediscovery of the doldrums in
501 storm-resolving simulations over the tropical Atlantic, *Nature Geoscience*, 10, 891, 2017.

502 Koren, I., Kaufman, Y. J., Rosenfeld, D., Remer, L. A., and Rudich, Y.: Aerosol invigoration
503 and restructuring of Atlantic convective clouds, *Geophysical Research Letters*, 32,
504 10.1029/2005gl023187, 2005.

505 Koren, I., Remer, L. A., Altaratz, O., Martins, J. V., and Davidi, A.: Aerosol-induced changes
506 of convective cloud anvils produce strong climate warming, *Atmospheric Chemistry and*
507 *Physics*, 10, 5001-5010, 10.5194/acp-10-5001-2010, 2010.

508 Koren, I., Dagan, G., and Altaratz, O.: From aerosol-limited to invigoration of warm
509 convective clouds, *science*, 344, 1143-1146, 2014.

510 Lebo, Z. J., and Morrison, H.: Dynamical effects of aerosol perturbations on simulated
511 idealized squall lines, *Monthly Weather Review*, 142, 991-1009, 2014.

512 Lee, S. S., Donner, L. J., and Phillips, V. T. J.: Sensitivity of aerosol and cloud effects on
513 radiation to cloud types: comparison between deep convective clouds and warm stratiform
514 clouds over one-day period, *Atmospheric Chemistry and Physics*, 9, 2555-2575, 2009.

515 Levin, Z., and Cotton, W. R.: *Aerosol pollution impact on precipitation: A scientific review*,
516 Springer, 2009.

517 Liu, H., Guo, J., Koren, I., Altaratz, O., Dagan, G., Wang, Y., Jiang, J. H., Zhai, P., and Yung,
518 Y. L.: Non-Monotonic Aerosol Effect on Precipitation in Convective Clouds over Tropical
519 Oceans, *Scientific Reports*, 9, 7809, 2019.

520 Malavelle, F. F., Haywood, J. M., Jones, A., Gettelman, A., Clarisse, L., Bauduin, S., Allan,
521 R. P., Karset, I. H. H., Kristjánsson, J. E., and Oreopoulos, L.: Strong constraints on aerosol–
522 cloud interactions from volcanic eruptions, *Nature*, 546, 485, 2017.

523 Medeiros, B., and Nuijens, L.: Clouds at Barbados are representative of clouds across the trade
524 wind regions in observations and climate models, *Proceedings of the National Academy of*
525 *Sciences*, 113, E3062-E3070, 2016.

526 Mlawer, E. J., Taubman, S. J., Brown, P. D., Iacono, M. J., and Clough, S. A.: Radiative
527 transfer for inhomogeneous atmospheres: RRTM, a validated correlated-k model for the
528 longwave, *Journal of Geophysical Research: Atmospheres*, 102, 16663-16682, 1997.

529 Mülmenstädt, J., and Feingold, G.: The Radiative Forcing of Aerosol–Cloud Interactions in
530 Liquid Clouds: Wrestling and Embracing Uncertainty, *Current Climate Change Reports*, 4, 23-
531 40, 2018.

532 Naumann AK, Kiemle C. The vertical structure and spatial variability of lower tropospheric
533 water vapor and clouds in the trades. *Atmospheric Chemistry and Physics*,
534 <https://doi.org/10.5194/acp-2019-1015> 2019.

535 Pinsky, M., Mazin, I., Korolev, A., and Khain, A.: Supersaturation and diffusional droplet
536 growth in liquid clouds, *Journal of the Atmospheric Sciences*, 70, 2778-2793, 2013.

537 Rosenfeld, D., Lohmann, U., Raga, G. B., O'Dowd, C. D., Kulmala, M., Fuzzi, S., Reissell, A.,
538 and Andreae, M. O.: Flood or drought: How do aerosols affect precipitation?, *Science*, 321,
539 1309-1313, 10.1126/science.1160606, 2008.

540 Rosenfeld, D., Wood, R., Donner, L. J., and Sherwood, S. C.: Aerosol cloud-mediated radiative
541 forcing: highly uncertain and opposite effects from shallow and deep clouds, in: *Climate*
542 *Science for Serving Society*, Springer, 105-149, 2013.

543 Rosenfeld, D., Zhu, Y., Wang, M., Zheng, Y., Goren, T., and Yu, S.: Aerosol-driven droplet
544 concentrations dominate coverage and water of oceanic low-level clouds, *Science*, 363,
545 eaav0566, 2019.

546 Rothenberg, D., Avramov, A., and Wang, C.: On the representation of aerosol activation and
547 its influence on model-derived estimates of the aerosol indirect effect, *Atmos. Chem. Phys*, 18,
548 7961-7983, 2018.

549 Seifert, A., and Beheng, K.: A two-moment cloud microphysics parameterization for mixed-
550 phase clouds. Part 2: Maritime vs. continental deep convective storms, *Meteorology and*
551 *Atmospheric Physics*, 92, 67-82, 2006a.

552 Seifert, A., and Beheng, K. D.: A two-moment cloud microphysics parameterization for mixed-
553 phase clouds. Part 1: Model description, *Meteorology and atmospheric physics*, 92, 45-66,
554 2006b.

555 Seifert, A., Heus, T., Pincus, R., and Stevens, B.: Large-eddy simulation of the transient and
556 near-equilibrium behavior of precipitating shallow convection, *Journal of Advances in*
557 *Modeling Earth Systems*, 2015.

558 Stevens, B., and Feingold, G.: Untangling aerosol effects on clouds and precipitation in a
559 buffered system, *Nature*, 461, 607-613, 10.1038/nature08281, 2009.

560 Stevens, B., Farrell, D., Hirsch, L., Jansen, F., Nuijens, L., Serikov, I., Brüggemann, B., Forde,
561 M., Linne, H., and Lonitz, K.: The Barbados Cloud Observatory: Anchoring investigations of
562 clouds and circulation on the edge of the ITCZ, *Bulletin of the American Meteorological*
563 *Society*, 97, 787-801, 2016.

564 Stevens, B., Ament, F., Bony, S., Crewell, S., Ewald, F., Gross, S., Hansen, A., Hirsch, L.,
565 Jacob, M., and Kölling, T.: A high-altitude long-range aircraft configured as a cloud
566 observatory—the NARVAL expeditions, *Bulletin of the American Meteorological Society*,
567 2019.

568 Storelvmo, T., Hoose, C., and Eriksson, P.: Global modeling of mixed-phase clouds: The
569 albedo and lifetime effects of aerosols, *Journal of Geophysical Research: Atmospheres*, 116,
570 2011.

571 Tao, W.-K., Chen, J.-P., Li, Z., Wang, C., and Zhang, C.: Impact of aerosols on convective
572 clouds and precipitation, *Reviews of Geophysics*, 50, RG2001, 2012.

573 Twomey, S.: The influence of pollution on the shortwave albedo of clouds, *Journal of the*
574 *atmospheric sciences*, 34, 1149-1152, 1977.

575 van den Heever, S. C., Stephens, G. L., and Wood, N. B.: Aerosol Indirect Effects on Tropical
576 Convection Characteristics under Conditions of Radiative-Convective Equilibrium, *Journal of*
577 *the Atmospheric Sciences*, 68, 699-718, 10.1175/2010jas3603.1, 2011.

578 Yamaguchi, T., Feingold, G., & Kazil, J. (2017). Stratocumulus to Cumulus Transition by
579 Drizzle. *Journal of Advances in Modeling Earth Systems*, 9(6), 2333-2349.
580 doi:10.1002/2017MS001104

581 Zängl, G., Reinert, D., Rípodas, P., and Baldauf, M.: The ICON (ICOsahedral Non-hydrostatic)
582 modelling framework of DWD and MPI-M: Description of the non-hydrostatic dynamical core,
583 *Quarterly Journal of the Royal Meteorological Society*, 141, 563-579, 2015.

584

585